Heme oxygenase limits mycobacterial infection-induced ferroptosis

Kaiming Luo[1,2], Roland Stocker[2,3], Warwick J Britton[1,4], Kazu Kikuchi[2,5], Stefan H Oehlers[1,6]

[1] Tuberculosis Research Program at the Centenary Institute, The University of Sydney, Camperdown, NSW 2050, Australia

[2] Victor Chang Cardiac Research Institute, Darlinghurst NSW 2010, Australia

[3] The Heart Research Institute, Newtown, NSW 2042, Australia

[4] Department of Clinical Immunology, Royal Prince Alfred Hospital, Camperdown, NSW 2050, Australia

[5] National Cerebral and Cardiovascular Center, Suita, Osaka 564-8565, Japan

[6] The University of Sydney, Discipline of Infectious Diseases & Immunology and Marie Bashir Institute, Camperdown, NSW 2006, Australia

Corresponding author email: stefan.oehlers@sydney.edu.au

Abstract

Iron homeostasis is essential for both sides of the host-pathogen interface. Restricting access of iron slows bacterial growth while iron is also a necessary co-factor for host immunity. Heme oxygenase 1 (HMOX1) is a critical regulator of iron homeostasis that catalyses the liberation of iron during degradation of heme. It is also a stress-responsive protein that can be rapidly upregulated and confers protection to the host. Although a protective role of HMOX1 has been demonstrated in a variety of diseases, the role of HMOX1 in *Mycobacterium tuberculosis* infection is equivocal across experiments with different host-pathogen combinations. Here we use the natural host-pathogen pairing of the zebrafish-*Mycobacterium marinum* infection platform to study the role of zebrafish heme oxygenase in mycobacterial infection. We identify zebrafish Hmox1a as the relevant functional paralog of mammalian HMOX1 and demonstrate a conserved role for Hmox1a in protecting the host

from mycobacterial infection. Using genetic and chemical tools, we show zebrafish Hmox1a protects the host against mycobacterial infection by reducing infection-induced iron accumulation and ferroptosis.

Keywords: Hmox1, mycobacteria, ferroptosis, iron, granuloma

Introduction

Infection with pathogenic mycobacteria, such as *Mycobacterium tuberculosis* (*Mtb*), leads to the formation of granulomas, the hallmark histological feature of tuberculosis (TB) [1]. Host cells within granulomas undergo significant phenotypic remodelling including the upregulation of cytoprotective stress response proteins in response to mycobacterial virulence factors and changes to the microenvironment [2-4].

Haem oxygenase 1 (HMOX1), a key regulator of iron homeostasis and cellular redox biology, is expressed within human- and mouse-*Mtb* granulomas [3-9]. HMOX1-derived carbon monoxide inhibits the growth of mycobacteria by direct toxicity and inducing mycobacterial dormancy gene expression [10-12]. HMOX1-deficient mice are more susceptible to mycobacterial infection, while inhibition of HMOX1 activity with tin protoporphyrin (SnPP) increases hosts resistance to mycobacterial infection in human macrophages and mouse models [3-5, 8-10, 13]. It is unclear if these contrasting effects on *Mtb* infection are a function of losing non-enzymatic HMOX1 functions in the gene deficient mice, differences in infection models, or other reasons [14].

HMOX1 is a highly evolutionarily conserved enzyme that has been identified in a wide variety of organisms. Zebrafish *hmox1a* and *hmox1b* encode paralogs of mammalian HMOX1, and their transcription is responsive to a range of oxidative stress-inducing conditions [15-17]. The zebrafish-*M. marinum* model has been widely used to study conserved host redox perturbations associated with

53 mycobacterial infection [18-20]. Here we have used zebrafish to investigate the role of Hmox1a in
54 the control of mycobacterial infection. We provide evidence that induction of host Hmox1a
55 expression restricts iron supply to limit mycobacterial growth and prevent excessive ferroptosis.
56
57 **Materials and Methods**
58 *Zebrafish husbandry*
59 Adult zebrafish were maintained at Centenary Institute and embryos were obtained by natural
60 spawning followed and raised in E3 media at 28-32°C (Sydney Local Health District AWC
61 Approvals: 16-037 and 17-036).
62
63 *M. marinum* infection
64 Single cell suspensions of mid log-phase fluorescent *M. marinum* strains and ΔESX1 *M. marinum*
65 were stored at -80°C in aliquots [21]. Zebrafish infections were carried out as previously described
66 with 200 CFU infection doses by microinjection into embryos or intraperitoneal injection into adults
67 [21, 22]. Infected adults were maintained at 28°C with 14:10 light:dark lighting cycle.
68
69 *Quantitative Real–time PCR*
70 Total RNA was extracted from homogenates using Trizol (Thermofisher) and cDNA was synthesised
71 with a High Capacity cDNA Synthesis Kit (Applied Biosystems). qPCR reactions were performed
72 on a LightCycler® 480 System. Gene expression was quantified by the delta–delta C_T method using
73 normalisation to zebrafish *bact* or *M. marinum 18s* as appropriate. Sequences of primers are listed in
74 Supplementary Table 1.
75
76 *Histology*
77 Cryosectioning was performed as previously described [22]. Hmox1 immunostaining was carried out
78 with a mouse anti-HMOX1 primary (GeneTex GTX633693) and a goat anti-mouse Alexa Fluor 488

79 (Thermofisher R37120). Perls' Prussian Blue staining was performed in acid ferrocyanide solution
80 (equal amount of 5% aqueous potassium ferrocyanide and 5% HCl) for 30 min at room temperature
81 followed by two washes of distilled water and counterstaining with 0.1% nuclear fast red. Whole
82 mount embryo Perls' Prussian Blue staining was performed without the counterstaining step.
83
84 *CRISPR/Cas9 Gene Editing Technique*
85 The gRNA target sites for each gene were designed using CRISPRscan. The sequences of gRNA
86 oligonucleotides are listed in Supplementary Table 2. The gRNA templates were amplified by PCR
87 with scaffold reverse primer, and then transcribed with HiScribe™ T7 High Yield RNA Synthesis
88 Kit (NEB) [23]. One cell stage embryos were injected with 1 nL of a mixture containing 200 ng/µL
89 of the four gRNAs and 2 ng/µL Cas9.
90
91 *Imaging*
92 Imaging was carried out on Leica M205FA and DM6000B, and Deltavision Elite microscopes as
93 previously described [18, 21, 22].
94
95 *Image analysis*
96 Fluorescent pixel count for enumeration of bacterial burden and quantification of fluorescent staining
97 was carried out as previously described in ImageJ [21]. Fluorescent stain areas are reported as pixels
98 per granuloma.
99
100 Perls' Prussian Blue staining in embryos was quantified by splitting the blue channel from colour
101 images and then using the "Measure" function in ImageJ to quantify the inverse mean pixel intensity
102 of a constant area within granulomas. The "average blue intensity per granuloma" was calculated by
103 subtracting the background blue pixel intensity from the granuloma blue pixel intensity.
104

105 *Whole mount in situ hybridisation*

106 Sequences of primers used to generate the DIG-labelled *hmox1a* probe are listed in Supplementary
107 Table 1, *in situ* hybridisation was carried out as previously described [24].

108

109 *Cell death and reactive oxygen species staining*

110 TUNEL and CellROX staining were performed as previously described and according to
111 manufacturer's instructions [18].

112

113 *Statistical analysis*

114 Student's *t* and ANOVA tests were carried out as appropriate for multiple comparisons using
115 Graphpad Prism. Each data point indicates a single animal unless otherwise stated. Data are plotted
116 as means +/- standard deviation.

117

118 **Results**

119 **Zebrafish *hmox1a* is the functional Hmox paralog in *M. marinum* infection**

120 Zebrafish have four Hmox-encoding paralogs: *hmox1a*, *hmox1b*, *hmox2a*, and *hmox2b* [15-17]. To
121 determine which paralog is functional in *M. marinum* infection, we first infected adult zebrafish by
122 intraperitoneal injection and analysed gene expression changes at 14 days post infection (dpi).
123 Infected adults had increased expression of *hmox1a*, but not the other paralogs (Fig. 1A).

124

125 To investigate the function of each paralog during *M. marinum* infection, we next used CRISPR/Cas9
126 technology to knockdown each paralog and infected crispant embryos with *M. marinum* (Fig. 1B).
127 Knockdown of *hmox1a* increased the bacterial burden at 5 dpi, while knockdown of *hmox1b*, *hmox2a*,
128 and *hmox2b* did not affect bacterial burden (Fig. 1C).

129

130 To investigate *hmox1a* expression in more detail, whole mount *in situ* hybridisation was used to
131 visualise the spatial distribution of *hmox1a* expression within *M. marinum*-infected embryos. *hmox1a*
132 was highly expressed in the haematopoietic niche of the caudal haematopoietic tissue and around
133 granulomas (Fig. 1D). To spatially examine Hmox expression in adult granulomas, we used a mouse
134 Hmox1 antibody which would potentially detect both Hmox1a and Hmox1b in zebrafish. Hmox1
135 staining was detected within the host cellular rim of granulomas from 14 dpi zebrafish adults (Fig.
136 1E).
137
138 **Hmox1a-dependent *M. marinum* granuloma formation does not explain increased susceptibility**
139 **to infection**
140 To investigate the function of *hmox1a* in the formation of adult zebrafish-*M. marinum* granulomas,
141 we utilised our *hmox1a*^{vcc42} knockout allele [25]. As expected from our CRISPR-Cas9 knockdown
142 studies, *hmox1a*$^{vcc42/vcc42}$ embryos displayed significantly increased bacterial burden compared to WT
143 clutch mates (Fig. 2A). Adult *hmox1a*$^{vcc42/vcc42}$ mutants had increased mortality following infection
144 that was consistent with the increased bacterial burden (Fig. 2B). Heterozygous *hmox1a*$^{+/vcc42}$
145 zebrafish displayed intermediate phenotypes in both assays (Fig. 2A and B).
146
147 Failure to form granulomas has been proposed to underly the mycobacterial control defect in *Hmox1*-
148 null mice [3, 4]. To determine if zebrafish reproduced this phenotype, we scored *M. marinum*
149 granulomas as "organised" or "loose" based on host nuclear structure in *hmox1a*$^{vcc42/vcc42}$ and their
150 WT clutch mates (Fig. 2C) [2, 22]. The proportion of unorganised "loose" granulomas in
151 *hmox1a*$^{vcc42/vcc42}$ adults was significantly higher than in the WT adults demonstrating a conserved
152 defect in granuloma formation (Fig. 2D).
153
154 To investigate the association between *hmox1a* and granuloma formation, we infected
155 *hmox1a*$^{vcc42/vcc42}$ embryos with ΔESX1 *M. marinum*, a strain that is unable to drive granuloma

156 formation [26]. Unexpectedly, ΔESX1 *M. marinum* load was significantly increased in
157 *hmox1a*$^{vcc42/vcc42}$ homozygous larvae at both 3 and 5 dpi suggesting a more general susceptibility to
158 mycobacterial infection than a defect in granuloma formation alone (Fig. 2E).
159
160 **Hmox1a restricts iron to control mycobacterial infection**
161 Since HMOX1 is a key regulator of iron homeostasis, we performed Perls' Prussian blue staining on
162 sections from WT and *hmox1a*$^{vcc42/vcc42}$ adults to visualise free iron (Fig. 3A). There were more Perls'
163 Prussian blue positive granulomas in *hmox1a*$^{vcc42/vcc42}$ mutants than WT zebrafish (Fig. 3B). Perls'
164 Prussian blue staining of *M. marinum*-infected embryos was not as vivid as that of adult granulomas
165 (Fig. 3C), but spectral quantification staining detected more Perls' Prussian blue staining in
166 granulomas from *hmox1a* crispants (Fig. 3D).
167
168 To confirm the presence of increased iron at the host-pathogen interface, we performed gene
169 expression analysis of *aco1*, a host iron-suppressed regulator of iron metabolism [27], which was
170 downregulated in 5 dpi *hmox1a*$^{vcc42/vcc42}$ embryos (Fig. 3E). To investigate the bacterial response, we
171 profiled the expression of *bfrB*, an iron storage gene in *M. marinum* homologous to human ferritin.
172 Expression of *bfrB* was progressively increased from 1 to 3 to 5 dpi and was higher in *hmox1a*
173 crispants than WT hosts at 5 dpi (Fig. 3F).
174
175 **Hmox1a-deficiency exposes hosts to infection-induced ferroptosis**
176 Mycobacteria require iron as a redox cofactor for vital enzymes and utilise multiple strategies to
177 acquire iron from the host [28, 29]. Excessive iron can be toxic to host cells by triggering ferroptosis,
178 a recently described mode of cell death associated with lipid peroxidation that drives pathology in the
179 mouse-*Mtb* model [30, 31]. We hypothesised ferroptosis could be responsible for the increased *M.*
180 *marinum* burden in our Hmox1a-deficent zebrafish.
181

182 Consistent with the increased iron in Hmox1a-deficient zebrafish, we observed increased granuloma
183 CellROX staining in *hmox1a* crispants compared to control embryos (Fig. 4A). We also observed
184 more TUNEL positive cells around granulomas in *hmox1a* crispants (Fig. 4B).
185
186 To test the role of ferroptosis in these phenotypes we treated embryos with ferrostatin, a small
187 molecule inhibitor of ferroptosis. Ferrostatin treatment reduced bacterial burden in *hmox1a* crispants
188 but not in scramble controls (Fig. 4C). Ferrostatin treatment also reduced CellROX staining in
189 granulomas and the number of TUNEL positive cells per granuloma (Fig 4D and 4E).
190
191 **Discussion**
192 Host cells need to balance iron availability and the production of reactive oxygen species during
193 infection with intracellular pathogens. Our data show infection-induced Hmox1a is a host-protective
194 enzyme that aids containment of infection within granulomas and slows the growth of mycobacteria
195 by restricting iron availability and preventing ferroptosis.
196
197 Our study clearly identifies zebrafish *hmox1a* as the functional ortholog of mammalian HMOX1 as
198 the most transcriptionally responsive to infection in adult zebrafish and the only gene which had a
199 knockdown burden phenotype in the CRIPSR-Cas9 embryo infection model. Our data further
200 suggests zebrafish *hmox1b* does not functionally compensate for loss of *hmox1a* and may be a
201 pseudogene.
202
203 Our experiment infecting *hmox1a*-deficient zebrafish with the ΔESX1 *M. marinum* suggests *hmox1a*
204 is involved in control of mycobacterial infection upstream of granuloma formation. We found iron
205 accumulation in mycobacterial granulomas which correlated with CellROX staining and increased
206 cell death in *hmox1a*-deficient zebrafish. These phenotypes were reversed after treatment with

207 ferrostatin suggesting the mycobacterial control defect in *hmox1a*-deficient zebrafish could be driven
208 by iron-induced ferroptosis upstream of granuloma formation.
209
210 The non-specific action of ferrostatin-1 is a potential limitation of our study. Ferrostatin-1 has been
211 recently reported to inhibit the enzymic activity of 15-Lipoxygenase, which produces the HpETE-PE
212 ferroptotic cell death signal as part of the 15LOX/PEBP1 complex with iron as a cofactor [32, 33].
213 Infection-induced lipoxygenase and cyclooxygenase activity in mycobacterial infection generally
214 leads to unfavourable suppression of inflammation, while inhibition of these enzyme families
215 generally controls mycobacterial infection [34-38]. Thus, we are unable to rule out 15LOX/PEBP1-
216 induced ferroptosis as a possible mechanism of ferrostatin-induced protection in our *hmox1a*-
217 deficient zebrafish.
218
219 The lack of host protection in WT embryos treated with ferrostatin suggests ferroptosis is of limited
220 importance in the zebrafish embryo-*M. marinum* infection model. Our data show that depletion of
221 Hmox1a is required to sensitise embryos to biologically significant levels of ferroptosis by impairing
222 endogenous iron metabolism.
223
224 The results from the infection time course highlights 3-5 dpi as a key window in *M. marinum* infection
225 when granulomas undergo extensive organisation and expansion. During this time period, host
226 *hmox1a* and bacterial *bfrB* are highly upregulated, and *hmox1a*-deficient zebrafish embryos develop
227 their conditional pathologies. Together, these data provide evidence of heme oxygenase function in
228 the race to acquire iron between host and mycobacterium during granuloma formation.
229
230 **Acknowledgements**
231 We thank Drs Elinor Hortle and Pradeep Cholan for zebrafish infection and analysis methods
232 training, Drs Angela Kurz and Kristina Jahn of Sydney Cytometry for assistance with imaging

233 equipment, the Victor Chang Cardiac Research Institute BioCORE staff for zebrafish maintenance,
234 members of the Tuberculosis Research Program at the Centenary Institute for helpful discussion.
235 Funding: This work was supported by a Chinese Scholarships Council Postgraduate Scholarship to
236 KL; the University of Sydney Fellowship G197581, NSW Ministry of Health under the NSW
237 Health Early-Mid Career Fellowships Scheme H18/31086 to SHO; the NHMRC Centre of Research
238 Excellence in Tuberculosis Control (APP1153493) to WJB.

239

240 **References**

241 1. Ramakrishnan, L., *Mycobacterium tuberculosis pathogenicity viewed through the lens of*
242 *molecular Koch's postulates.* Curr Opin Microbiol, 2020. **54**: p. 103-110.
243 2. Cronan, M.R., et al., *Macrophage Epithelial Reprogramming Underlies Mycobacterial*
244 *Granuloma Formation and Promotes Infection.* Immunity, 2016. **45**(4): p. 861-876.
245 3. Regev, D., et al., *Heme oxygenase-1 promotes granuloma development and protects against*
246 *dissemination of mycobacteria.* Lab Invest, 2012. **92**(11): p. 1541-52.
247 4. Silva-Gomes, S., et al., *Heme catabolism by heme oxygenase-1 confers host resistance to*
248 *Mycobacterium infection.* Infect Immun, 2013. **81**(7): p. 2536-45.
249 5. Costa, D.L., et al., *Pharmacological Inhibition of Host Heme Oxygenase-1 Suppresses*
250 *Mycobacterium tuberculosis Infection In Vivo by a Mechanism Dependent on T*
251 *Lymphocytes.* MBio, 2016. **7**(5).
252 6. Abdalla, M.Y., et al., *Induction of heme oxygenase-1 contributes to survival of*
253 *Mycobacterium abscessus in human macrophages-like THP-1 cells.* Redox Biol, 2015. **4**: p.
254 328-39.
255 7. Rockwood, N., et al., *Mycobacterium tuberculosis Induction of Heme Oxygenase-1*
256 *Expression Is Dependent on Oxidative Stress and Reflects Treatment Outcomes.* Front
257 Immunol, 2017. **8**: p. 542.
258 8. Chinta, K.C., et al., *Microanatomic Distribution of Myeloid Heme Oxygenase-1 Protects*
259 *against Free Radical-Mediated Immunopathology in Human Tuberculosis.* Cell Rep, 2018.
260 **25**(7): p. 1938-1952 e5.
261 9. Scharn, C.R., et al., *Heme Oxygenase-1 Regulates Inflammation and Mycobacterial Survival*
262 *in Human Macrophages during Mycobacterium tuberculosis Infection.* J Immunol, 2016.
263 **196**(11): p. 4641-9.
264 10. Shiloh, M.U., P. Manzanillo, and J.S. Cox, *Mycobacterium tuberculosis senses host-derived*
265 *carbon monoxide during macrophage infection.* Cell Host Microbe, 2008. **3**(5): p. 323-30.
266 11. Kumar, A., et al., *Heme oxygenase-1-derived carbon monoxide induces the Mycobacterium*
267 *tuberculosis dormancy regulon.* J Biol Chem, 2008. **283**(26): p. 18032-9.
268 12. Zacharia, V.M., et al., *cor, a novel carbon monoxide resistance gene, is essential for*
269 *Mycobacterium tuberculosis pathogenesis.* mBio, 2013. **4**(6): p. e00721-13.
270 13. Costa, D.L., et al., *Heme oxygenase-1 inhibition promotes IFNgamma- and NOS2-mediated*
271 *control of Mycobacterium tuberculosis infection.* Mucosal Immunol, 2021. **14**(1): p. 253-
272 266.
273 14. Costa, D.L., et al., *Modulation of Inflammation and Immune Responses by Heme*
274 *Oxygenase-1: Implications for Infection with Intracellular Pathogens.* Antioxidants (Basel),
275 2020. **9**(12).

15. Mills, M.G. and E.P. Gallagher, *A targeted gene expression platform allows for rapid analysis of chemical-induced antioxidant mRNA expression in zebrafish larvae.* PLoS One, 2017. **12**(2): p. e0171025.
16. Holowiecki, A., B. O'Shields, and M.J. Jenny, *Spatiotemporal expression and transcriptional regulation of heme oxygenase and biliverdin reductase genes in zebrafish (Danio rerio) suggest novel roles during early developmental periods of heightened oxidative stress.* Comp Biochem Physiol C Toxicol Pharmacol, 2017. **191**: p. 138-151.
17. Holowiecki, A., B. O'Shields, and M.J. Jenny, *Characterization of heme oxygenase and biliverdin reductase gene expression in zebrafish (Danio rerio): Basal expression and response to pro-oxidant exposures.* Toxicol Appl Pharmacol, 2016. **311**: p. 74-87.
18. Black, H.D., et al., *The cyclic nitroxide antioxidant 4-methoxy-TEMPO decreases mycobacterial burden in vivo through host and bacterial targets.* Free Radic Biol Med, 2019. **135**: p. 157-166.
19. Roca, F.J. and L. Ramakrishnan, *TNF Dually Mediates Resistance and Susceptibility to Mycobacteria via Mitochondrial Reactive Oxygen Species.* Cell, 2013. **153**(3): p. 521-34.
20. Roca, F.J., et al., *TNF Induces Pathogenic Programmed Macrophage Necrosis in Tuberculosis through a Mitochondrial-Lysosomal-Endoplasmic Reticulum Circuit.* Cell, 2019. **178**(6): p. 1344-1361 e11.
21. Matty, M.A., S.H. Oehlers, and D.M. Tobin, *Live Imaging of Host-Pathogen Interactions in Zebrafish Larvae.* Methods Mol Biol, 2016. **1451**: p. 207-23.
22. Cheng, T., et al., *High content analysis of granuloma histology and neutrophilic inflammation in adult zebrafish infected with Mycobacterium marinum.* Micron, 2020. **129**: p. 102782.
23. Wu, R.S., et al., *A Rapid Method for Directed Gene Knockout for Screening in G0 Zebrafish.* Dev Cell, 2018. **46**(1): p. 112-125 e4.
24. Thisse, C. and B. Thisse, *High-resolution in situ hybridization to whole-mount zebrafish embryos.* Nat Protoc, 2008. **3**(1): p. 59-69.
25. Luo, K., et al., *Zebrafish heme oxygenase 1a is necessary for normal development and macrophage migration.* bioRxiv, 2021: p. 2021.04.07.438802.
26. Volkman, H.E., et al., *Tuberculous granuloma formation is enhanced by a mycobacterium virulence determinant.* PLoS Biol, 2004. **2**(11): p. e367.
27. Pantopoulos, K., *Iron metabolism and the IRE/IRP regulatory system: an update.* Ann N Y Acad Sci, 2004. **1012**: p. 1-13.
28. Marcela Rodriguez, G. and O. Neyrolles, *Metallobiology of Tuberculosis.* Microbiol Spectr, 2014. **2**(3).
29. Pandey, R. and G.M. Rodriguez, *A ferritin mutant of Mycobacterium tuberculosis is highly susceptible to killing by antibiotics and is unable to establish a chronic infection in mice.* Infect Immun, 2012. **80**(10): p. 3650-9.
30. Amaral, E.P., et al., *A major role for ferroptosis in Mycobacterium tuberculosis-induced cell death and tissue necrosis.* J Exp Med, 2019. **216**(3): p. 556-570.
31. Dixon, S.J., et al., *Ferroptosis: an iron-dependent form of nonapoptotic cell death.* Cell, 2012. **149**(5): p. 1060-72.
32. Anthonymuthu, T.S., et al., *Resolving the paradox of ferroptotic cell death: Ferrostatin-1 binds to 15LOX/PEBP1 complex, suppresses generation of peroxidized ETE-PE, and protects against ferroptosis.* Redox Biol, 2021. **38**: p. 101744.
33. Kagan, V.E., et al., *Oxidized arachidonic and adrenic PEs navigate cells to ferroptosis.* Nat Chem Biol, 2017. **13**(1): p. 81-90.
34. Hortle, E., et al., *Thrombocyte Inhibition Restores Protective Immunity to Mycobacterial Infection in Zebrafish.* J Infect Dis, 2019. **220**(3): p. 524-534.
35. Bafica, A., et al., *Host control of Mycobacterium tuberculosis is regulated by 5-lipoxygenase-dependent lipoxin production.* J Clin Invest, 2005. **115**(6): p. 1601-6.

36. Chen, M., et al., *Lipid mediators in innate immunity against tuberculosis: opposing roles of PGE2 and LXA4 in the induction of macrophage death.* J Exp Med, 2008. **205**(12): p. 2791-801.
37. Lewis, A. and P.M. Elks, *Hypoxia Induces Macrophage tnfa Expression via Cyclooxygenase and Prostaglandin E2 in vivo.* Front Immunol, 2019. **10**: p. 2321.
38. Tobin, D.M., et al., *Host genotype-specific therapies can optimize the inflammatory response to mycobacterial infections.* Cell, 2012. **148**(3): p. 434-46.

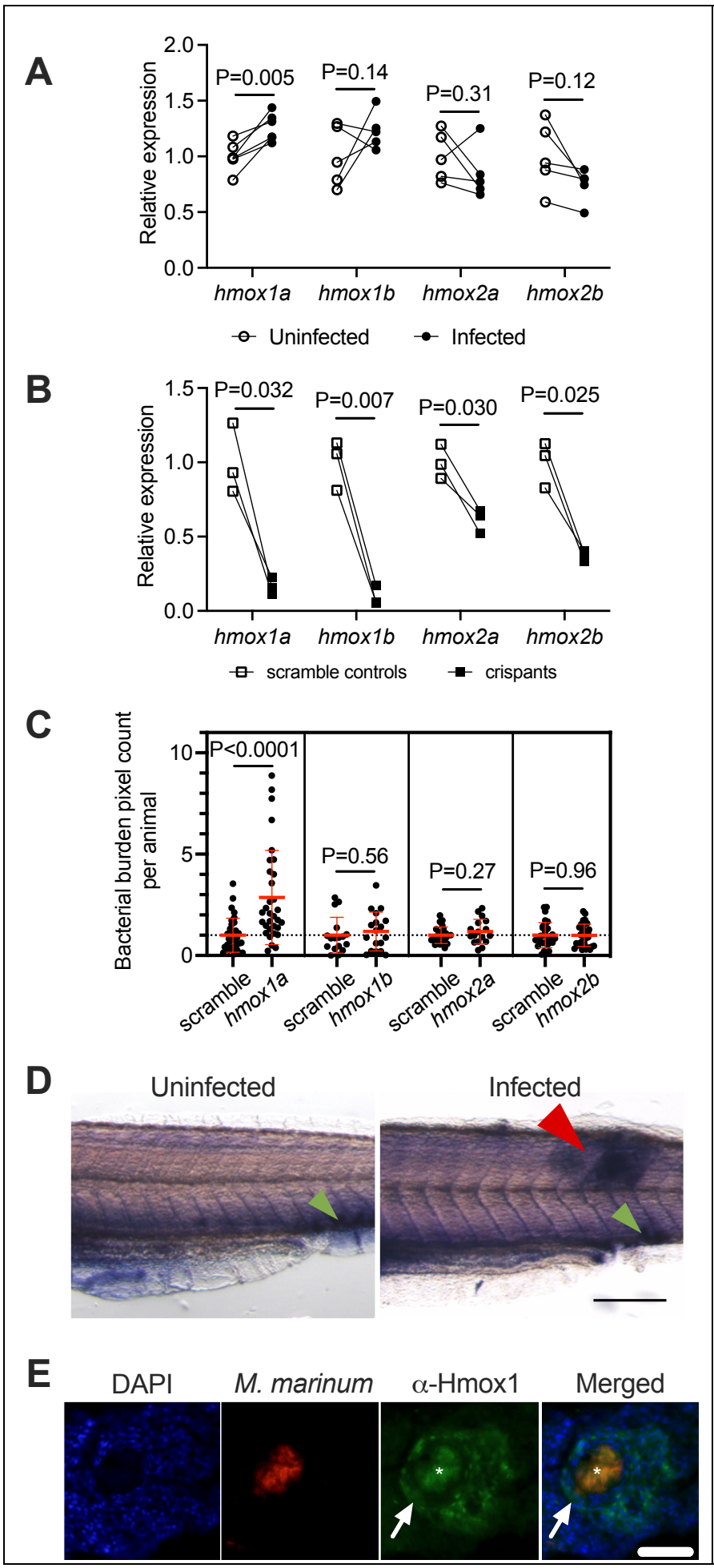

Figure 1: Zebrafish *hmox1a* is the functional paralog of mammalian *HMOX1* during mycobacterial infection
A. qPCR expression analysis of zebrafish *hmox* paralogs in homogenates of 14 dpi adult zebrafish infected with *M. marinum*. Biological pairs indicated by matching lines.
B. qPCR expression analysis of zebrafish *hmox* paralogs in 7 dpf crispants. Biological pairs indicated by matching lines.
C. *M. marinum* burden measured by fluorescent pixel count in 5 dpi crispants.
D. Whole mount *in situ* hybridisation detection of *hmox1a* transcripts in 5 dpi zebrafish embryos. Green arrowhead indicates site of constitutive CHT expression, red arrowhead indicates site of inducible expression at a granuloma. Scale bar represents 200 µm.
E. Representative image of antibody detection of Hmox1 in a granuloma of a 14 dpi adult zebrafish. Arrows indicate cellular rim of granuloma. Asterisk indicates bleed through fluorescence of *M. marinum*-TdTomato signal in necrotic core. Scale bar represents 100 µm.

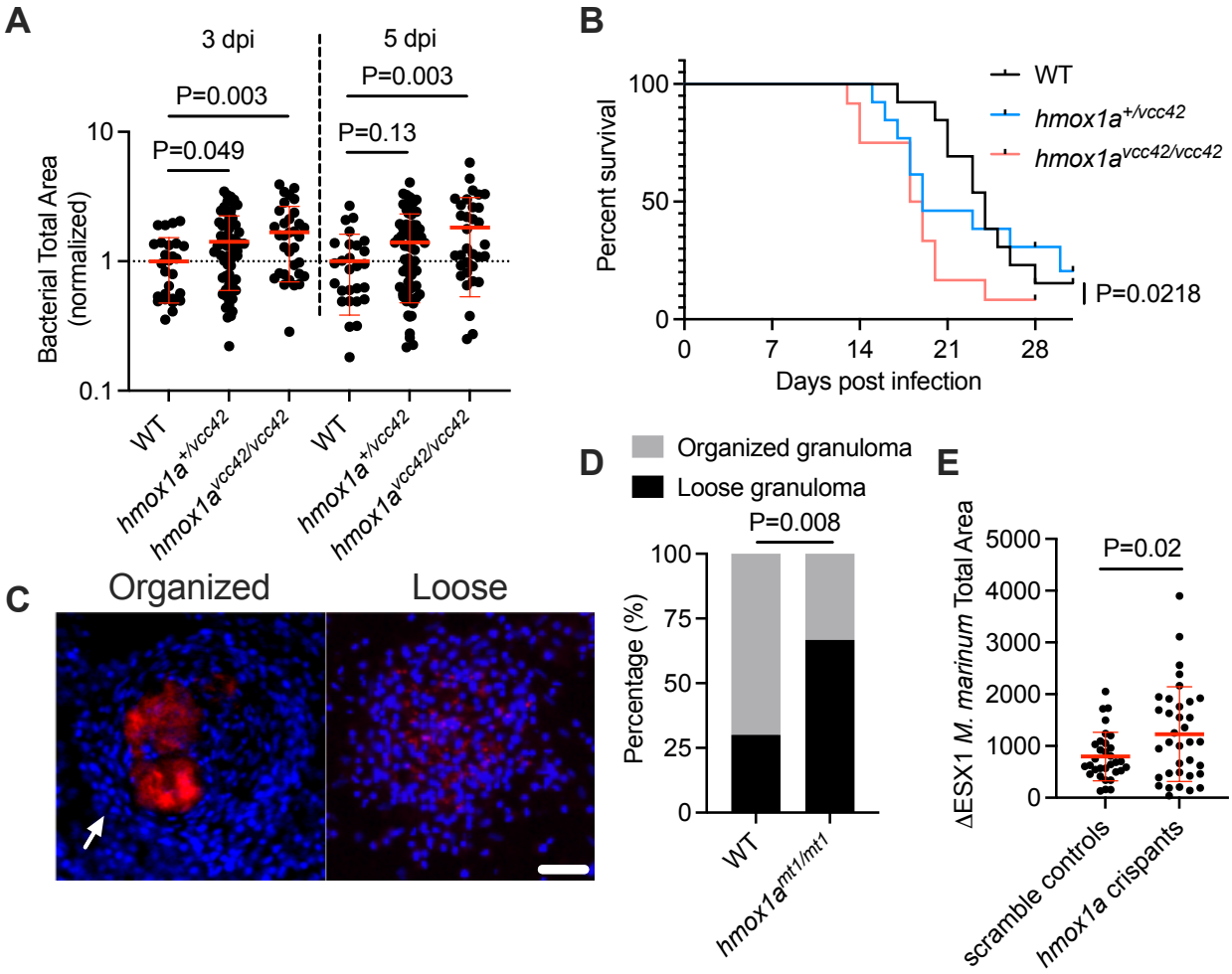

Figure 2: Zebrafish Hmox1a is necessary for efficient granuloma formation

A. Bacterial burden in 5 dpi *hmox1a*$^{vcc41/vcc42}$ mutant embryos.

B. Survival of adult *hmox1a*$^{vcc41/vcc42}$ mutant zebrafish following infection with *M. marinum*. n=13 WT, 13 heterozygous mutants, 12 homozygous mutants.

C. Representative images of granuloma morphology classes in 14 dpi *hmox1a*$^{vcc41/vcc42}$ mutant adult zebrafish. Arrow indicates organised cellular rim of granuloma. Scale bar represents 50 µm.

D. Quantification of granuloma morphology classes in 14 dpi *hmox1a*$^{vcc41/vcc42}$ mutant adult zebrafish. n = 40 WT granulomas from 3 animals, 24 *hmox1a*$^{vcc41/vcc42}$ mutant granulomas from 3 animals.

E. Bacterial burden in *hmox1a* crispants infected with ΔESX1 *M. marinum*.

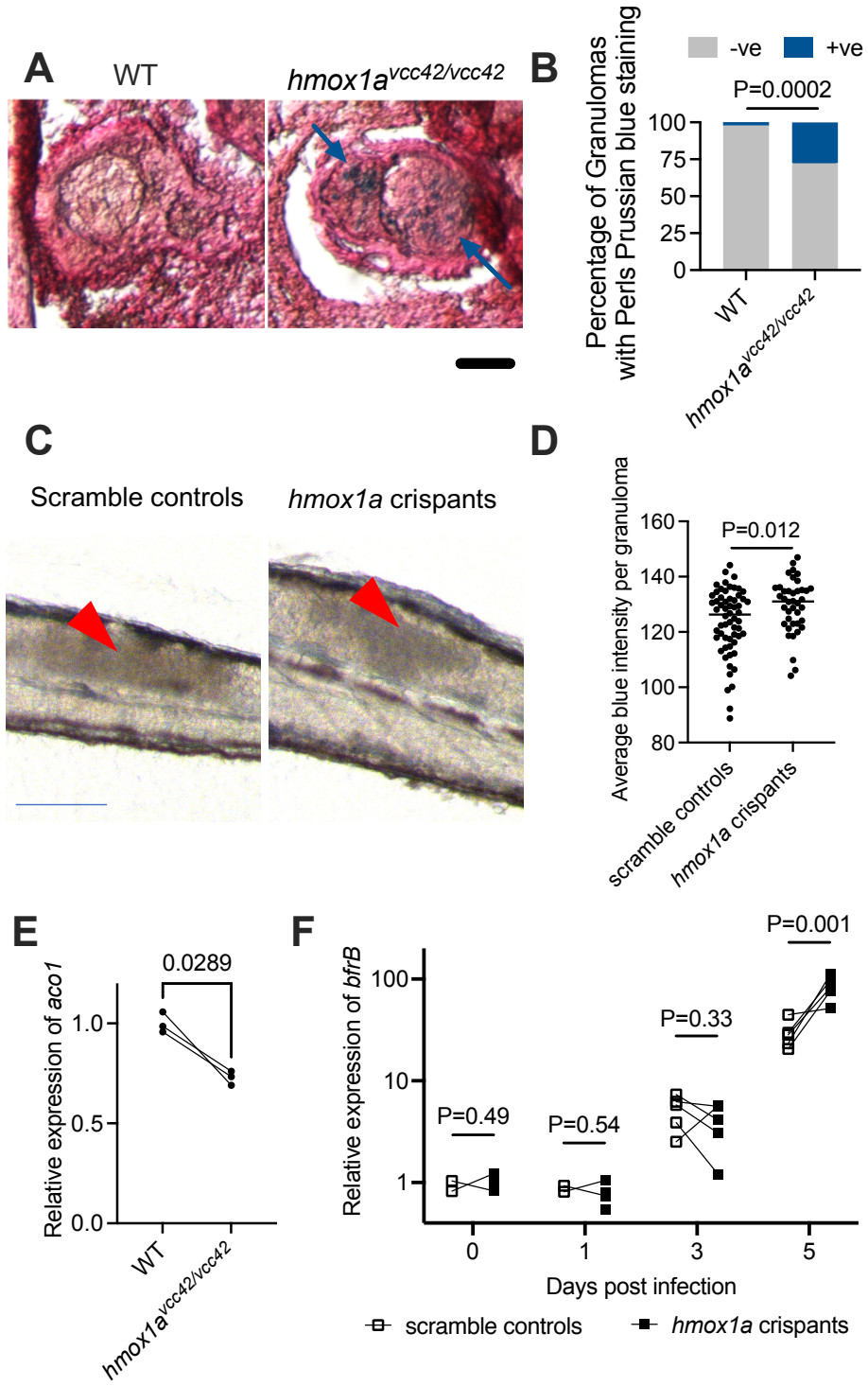

Figure 3: Zebrafish Hmox1a restricts iron availability during infection

A. Representative images of Perls' Prussian blue staining of granulomas from 14 dpi *hmox1a*$^{vcc41/vcc42}$ mutant adult zebrafish. Blue arrows indicate location of positive staining. Scale bar represents 50 µm.

B. Quantification of granuloma Perls' Prussian blue staining in *hmox1a*$^{vcc41/vcc42}$ mutant adult zebrafish. n = 46 granulomas from 3 WT animals, 83 granulomas from 3 *hmox1a*$^{vcc41/vcc42}$ mutants.

C. Representative images of Perls' Prussian blue staining of 5 dpi zebrafish embryos. Red arrows indicate locations of analysed granulomas. Scale bar represents 100 µm.

D. Quantification of granuloma Perls' Prussian blue staining in 5 dpi *hmox1a* crispants. Each data point represents a single granuloma from an individual embryo.

E. qPCR analysis of host *aco1* gene expression in 5 dpi *hmox1a*$^{vcc41/vcc42}$ mutant embryos.

F. qPCR analysis of *M. marinum bfrB* gene expression in *hmox1a* crispants.

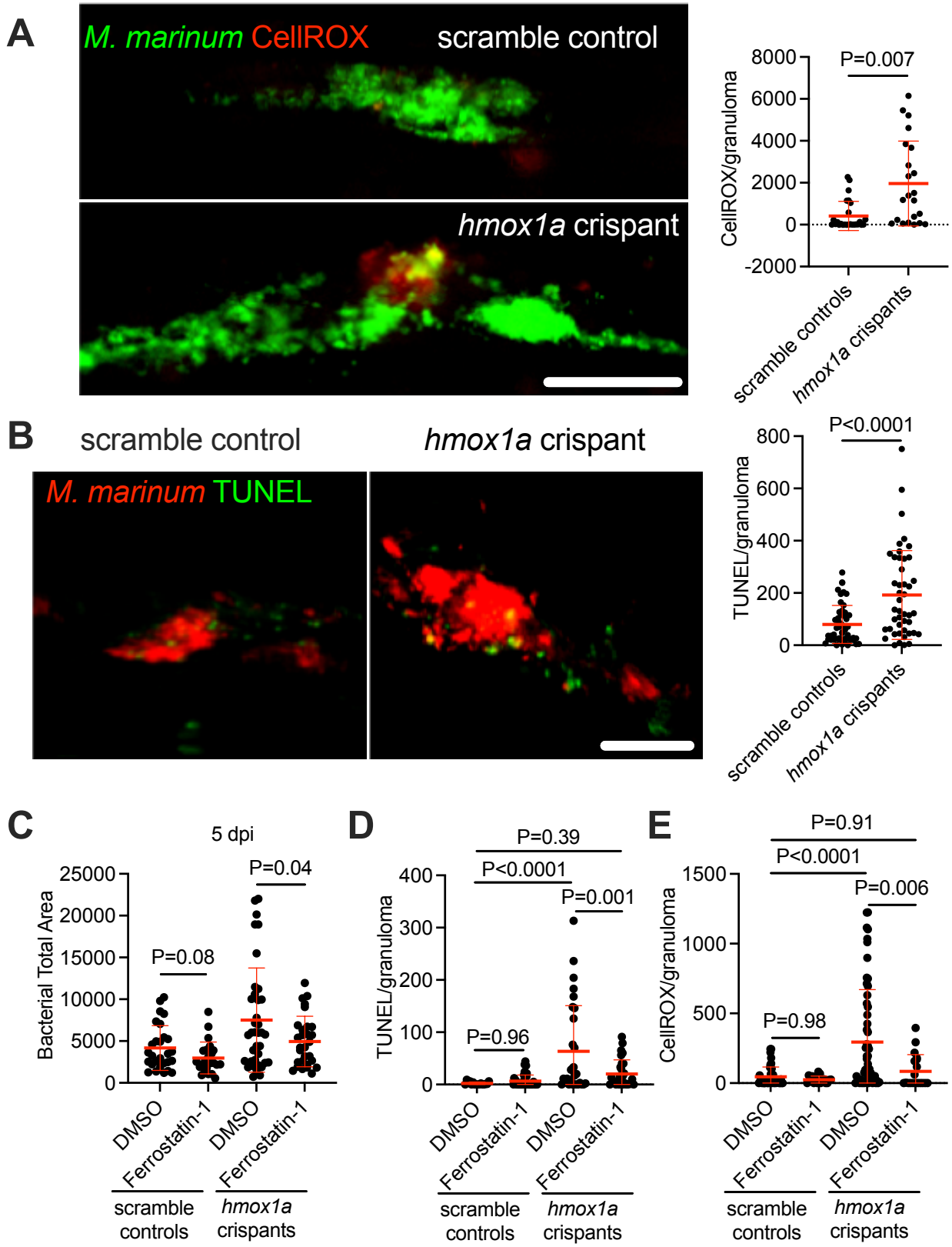

Figure 4: Zebrafish Hmox1a prevents infection-induced ferroptosis

A. Representative images and quantification of CellROX staining in 5 dpi *hmox1a* crispants. Scale bar represents 50 µm.

B. Representative images and quantification of TUNEL staining in 5 dpi *hmox1a* crispants. Scale bar represents 50 µm.

C. Bacterial burden in 5 dpi *hmox1a* crispants treated with ferrostatin-1.

D. Quantification of CellROX staining in 5 dpi *hmox1a* crispants treated with ferrostatin-1.

E. Quantification of TUNEL staining in 5 dpi *hmox1a* crispants treated with ferrostatin-1.